The ALS interferometric microscope upgraded for measurements with large x-ray optics and optical assemblies

Ian Lacey*[a], Kevan Anderson[b], Harold Barnard[a], Damon English[b], Wayne R. McKinney[c], Muhammad A. Saeed[d], and Valeriy V. Yashchuk[a]
[a]Advanced Light Source, Lawrence Berkeley National Laboratory, Berkeley, CA USA, 94720;
[d]Engineering Division, Lawrence Berkeley National Laboratory, Berkeley, CA USA, 94720;
[c]Dept. of Optics, Central Univ./City Branch, 9876 Light Ave., Philadelphia, PA USA 00555-9642;
[d]Physics Dept., California State Univ., East Bay, 25800 Carlos Bee Blvd. Hayward, CA USA 94542

ABSTRACT

We describe details of a recent deep upgrade of the MicroMap-570 interferometric microscope available at the Advanced Light Source X-Ray Optics Laboratory. The upgrade has included an improvement of the microscope optical sensor and data acquisition software, design and implementation of automated optic alignment and microscope translation systems, and development of a specialized software for data processing in the spatial frequency domain. With the upgraded microscope, we are now capable for automated (remoted) measurements with large x-ray optics and optical systems. The results of experimental evaluation of the upgraded microscope performance and calibration of its instrument transfer function are also discussed. Because the same already obsolete MicroMap-570 microscopes have been used for years at other metrology laboratories at the x-ray facilities around the globe, we believe that our experience on upgrade of the microscope describe in detail in the present paper is broadly interesting and useful.

Keywords: x-ray optical metrology, white-light interferometry, microscopy, form factor measurement, surface metrology

1. INTRODUCTION

Besides Angstrom-level accuracy (see, for example, Refs. [1-5] and references therein), interferometric microscopes, for use to characterize the surface topography of x-ray optics at the middle spatial frequencies (aka the surface finish [6-10]), have to fulfill specific requirements determined by the grazing incidence beamline applications of the optics. At the characteristic grazing incidence angles, between a couple to a few dozens of milliradians [11,12], the size of the clear aperture of the x-ray optics can be up to a meter in the tangential direction at a relatively small size in the sagittal direction. An appropriate microscope should be capable for measurements not only of the long bare optical substrate, but also of the assembled optic including the mechanical support and adjustment systems. However, most, if not all, available industrial interferometric microscopes are designed for measurements with relatively small optics and, therefore, are not capable for metrology with assembled x-ray optics.

In this respect, the MicroMap-570 interferometric microscope available at the Advanced Light Source (ALS) X-Ray Optics Laboratory (XROL) [13,14] is a rare exception. The flexible design of the microscope allows for easy accommodation of the tool to very different measurement arrangements. Figure 1 illustrates the application of the MicroMap-570 microscope to the surface topography measurements with an assembly of a bendable toroidal x-ray mirror. The mirror is under surface characterization because of a contamination that appeared after the mirror was in beamline operation for a few years. The contamination is seen in the right-hand picture in Fig. 1 as a white stripe along the mirror clear aperture in the tangential direction.

For many years, the ALS XROL MicroMap-570 interferometric microscope in its original design has been used for characterization of a broad spectrum of the ALS beamline optics [15-17]. Unfortunately, recently, the already obsolete microscope suffered a malfunction. By that time, the tool's vendor has left the market. To the best of our knowledge, a similar problem has persisted at other metrology laboratories at x-ray facilities around the globe, where MicroMap-570 microscopes have been used for years. Therefore, we believe that our experience on upgrade of the microscope described in detail in the present paper is broadly interesting and useful.

*ilacey@lbl.gov; phone 1 510 486-4117; https://als.lbl.gov

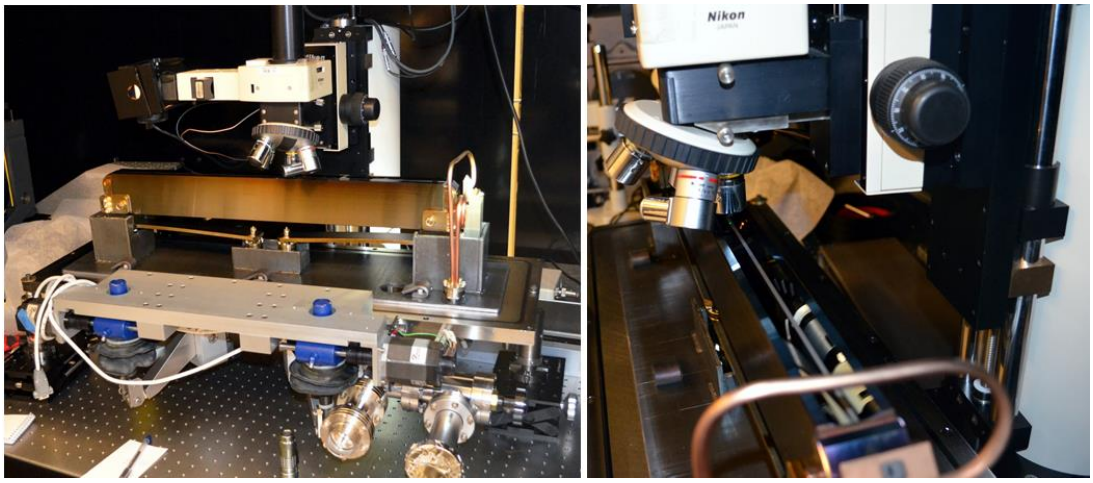

Figure 1. The ALS XROL MicroMap-570 interferometric microscope arranged for surface topography measurements with an assembly of a bendable toroidal x-ray mirror with the substrate length of ~ 880 mm. After operation at a beamline for a few years, the mirror surface appears to be contaminated as seen in the right-hand picture with a white stripe along the mirror clear aperture in the tangential direction. Photos were taken the ALS XROL in 2016.

The upgrade has included an improvement of the microscope's optical sensor and data acquisition software (see Sec. 2), design and implementation of automated optical alignment, microscope translation systems (Sec. 3), and (Sec. 4) development of specialized software for data processing in the spatial frequency domain. The results of experimental evaluation of the upgraded microscope performance and calibration of its instrument transfer function are also discussed (Sec. 5). With the upgraded microscope, we are now capable for automated (remote) measurements with large x-ray optics and optical systems (see discussion in Sec. 6).

2. UPGRADE OF MICROMAP-570 MICROSCOPE TO OPTOSURF

2.1 Upgrade of the microscope's optical sensor

The replacement of the objective's PZT system with the congruous OptoSURF parts [18] was performed by Eotech in Marcoussis, France. The parts then shipped back to the ALS, and commissioned on site.

The microscope's updated detector CCD camera has 778 × 578 pixels. Unlike the original camera, there is not the lateral resolution asymmetry, characteristic of the original MicroMap-570 detector see Ref. [15].

Figure 2 shows the upgraded ALS XROL MicroMap/OptoSURF interferometric microscope now in use at ALS XROL. Here, the microscope is arranged for the instrument transfer function (ITF) measurements with a binary pseudo-random array (BPRA) standard [19-25] (for more details, see also Sec. 5).

2.2 Upgrade of the microscope's control system and data acquisition and pre-processing software

The MicroMap-570 microscope control system has been substituted with that of the OptoSURF using its congruous parts. Both the PZT motion and lamp intensity are controlled by a standalone driver box with USB connections to the acquisition computer.

The camera shutter speed is used to adjust the recorded intensity of the interference fringes, depending on the numerical aperture of the objective and the reflectivity of the surface. Correspondingly, the OptoSURF software is adapted for data acquisition and pre-processing.

Figure 3 depicts a screenshot of the MicroMap/OptoSURF control and data acquisition and pre-processing software as it appears in the course of measurements with a test sample. The left pane shows the contrast image on the detector, the center lists the history of measurements within the operating session, and the right shows the height topography; in this case for a cylindrical x-ray substrate with 120 m ROC.

Figure 2. Upgraded MicroMap/OptoSURF interferometric microscope as arranged for the instrument transfer function (ITF) measurements (see Sec. 5) using a Binary Pseudo-Random Array (BPRA) calibration standard [19-25].

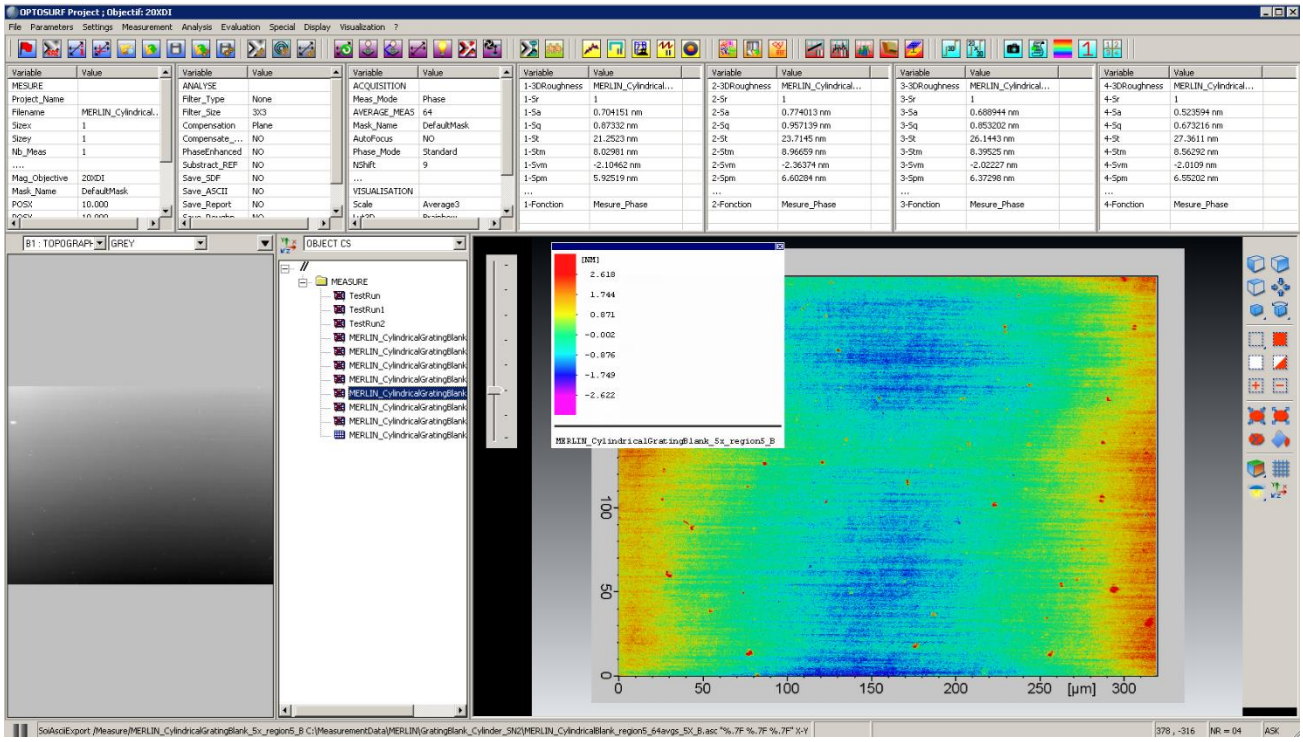

Figure 3. Screenshot of the MicroMap/OptoSURF control and data acquisition and pre-processing software. as it appears in the course of measurements with a test sample; in this case a cylindrical grating blank for potential use in the ALS BL 4.0.3.

3. REMOTE MOTION CONTROL AND DATA AQUISITION

The optical sensor of the upgraded MicroMap/OptoSURF microscope is mounted on the original MicroMap-570 ceramic tower with a manual lifting system normally used for a manual vertical translation of the sensor (coarse translation) and for fine tuning of the microscope focus (precise translation). In this case, the angular alignment of the optic under test (*aka* the surface under test, SUT) was performed with an additional kinematic stage.

In this section, we describe the upgrades of the microscope that allows remote control of the motion and data acquisition with automated control of the microscope longitudinal translation and fine angular alignment of the SUT.

3.1 Longitudinal translation of the microscope's optical sensor

In order to provide an automated translation of the MicroMap/OptoSURF microscope sensor mounted on the ceramic tower along a large sized x-ray mirror or mirror assembly, we use a linear translation stage [26] – Fig. 4a. The linear stage with carriage is used to ensure smooth, stable, and accurate longitudinal motion of the upgraded microscope. Position feedback is determined with an incremental encoder reading a grating strip along the side of the stage. The stage can translate the microscope head ~900 mm with positioning accuracy of a few microns. The motion control system of the stage is operated with the specially developed LabView software.

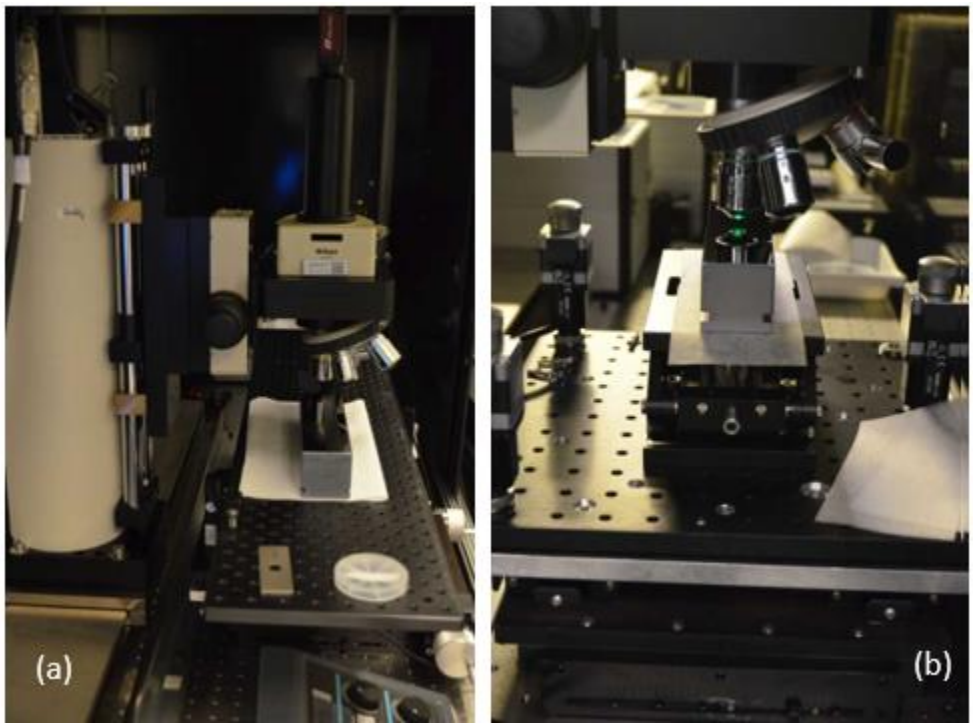

Figure 4. The upgraded MicroMap/OptoSURF interferometric microscope as mounted on (a) the American Linear Manufacturers linear translation stage [26]. (b) The automated kinematic stage developed for remote aligning and focusing the SUT (Sec. 3.2).

3.2 Automated kinematic stage for alignment and focus adjustment of the optic under test

The customized angular alignment kinematic stage (Fig. 4b) utilizes three high-load stepper motors [27] capable of supporting ~50 kg of balanced load with 8 mm adjustment range and 5 micron accuracy. Note that the absolute position accuracy of the motors is not important, since the parameter of merit is the interference fringes on the detector. This kinematic platform allows nulling of the fringes on the detector as different regions of a curved surface are under the field of view during the course of an effective scan of an x-ray mirror surface.

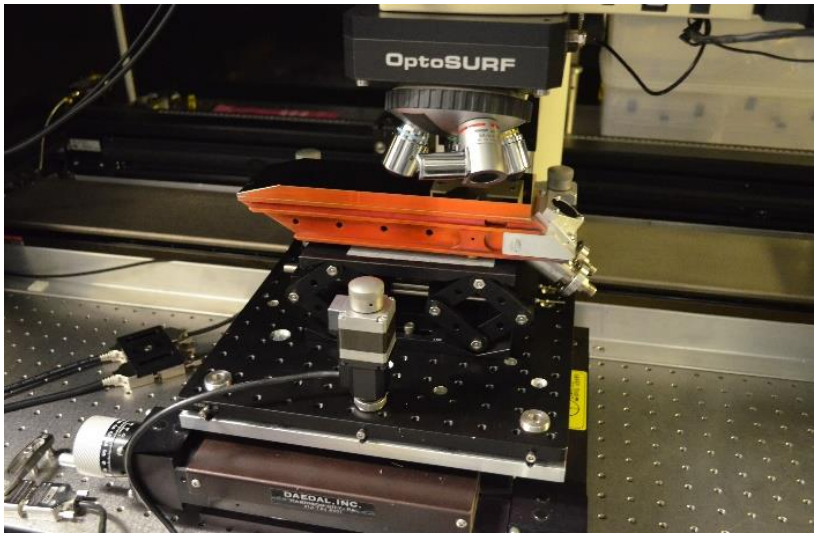

Figure 5. The developed angular alignment kinematic stage in use to inspect the line density of a water-cooled spherical grating.

The native OptoSURF software is adapted for data acquisition and pre-processing allowing verification of acquisition and a first-order inspection of surface features. More sophisticated processing, including analysis of the spatial frequency PSD, averaging, differences, and stitching is left for off-line post-processing.

4. CUSTOM DATA PROCESSING SOFTWARE

In addition to the native software format, the instrument can also export a table of pixel locations with corresponding height values. While the native format is encoded to take less hard drive space, the ASCII 'x-y-z' table of values is readily portable to any other common image data format for offline processing and analysis. For our purposes this is necessary so that we can perform in-house round-robin comparisons of surface data [15], either with a different interferometric microscope or with Fizeau interferometer data, as well as consider other non-standard processing functionality.

With the raw data in hand, we can consider specific processing relevant for the x-ray optics with which we work. In addition to rms roughness, we are typically concerned with the PSD of the surface [16, 28].

4.1 Specification of x-ray optics in terms of the power spectral density

The interferometric microscope, such as the upgraded MicroMap-570 / OptoSURF described here, has become a basic metrology tool for highly accurate testing of the surface finish of x-ray optics with sub-Angstrom rms roughness. The standard list of output parameters of an interferometric microscope measurement includes values of roughness averaged over an area and along a sample line. However, the task of designing high performance low scatter X-ray optical systems [4] requires the development of sophisticated X-ray scattering calculations based on rigorous information about the optics. One of the most insightful approaches to these calculations is based on the two-dimensional (2D) PSD distribution of the surface height,[3] allowing for the evaluation of three-dimensional distributions of x-rays scattered by the optics [5]. As a first step in designing custom software to process the data from the upgraded instrument, we have implemented the straightforward one-dimensional (1D) PSD, averaged in the two tangential directions:

$$\mathrm{PSD}(f) = \frac{2\,d_o}{N}\left|\sum_{n=1}^{N} e^{\frac{2\pi i}{N}(n-1)(m-1)}\, z(n)\right|^2 . \qquad (1)$$

Where $z(n)$ is the surface height as measured corresponding to a line of pixels in a 2D array, and $f = \frac{m-1}{Nd_0}$, where f varies from $1/L$ to $N/2L$. (we assume an even number of points in the line of data.) d_0 is the spacing of the pixels when mapped onto the surface.

4.2 Custom software for data processing in spatial frequency domain

Due to the migration of many labs, including LBNL away from proprietary developmental software platforms towards open source software the new PSD program was developed using the 64-bit Anaconda distribution of Python 3 on a 64-bit Windows computer within the Spyder 4 development environment. For ease of use, a graphical user interface (GUI) was created using PYQT5 [29]. Tkinter was investigated for use for the GUI in the beginning, but was abandoned as too cumbersome.

Figure 6 depicts a screenshot of the developed data processing software as it appears in the course of the PSD evaluation based on the ITF calibration measurements with the BPRA standard in the experimental arrangement depicted in Fig. 2.

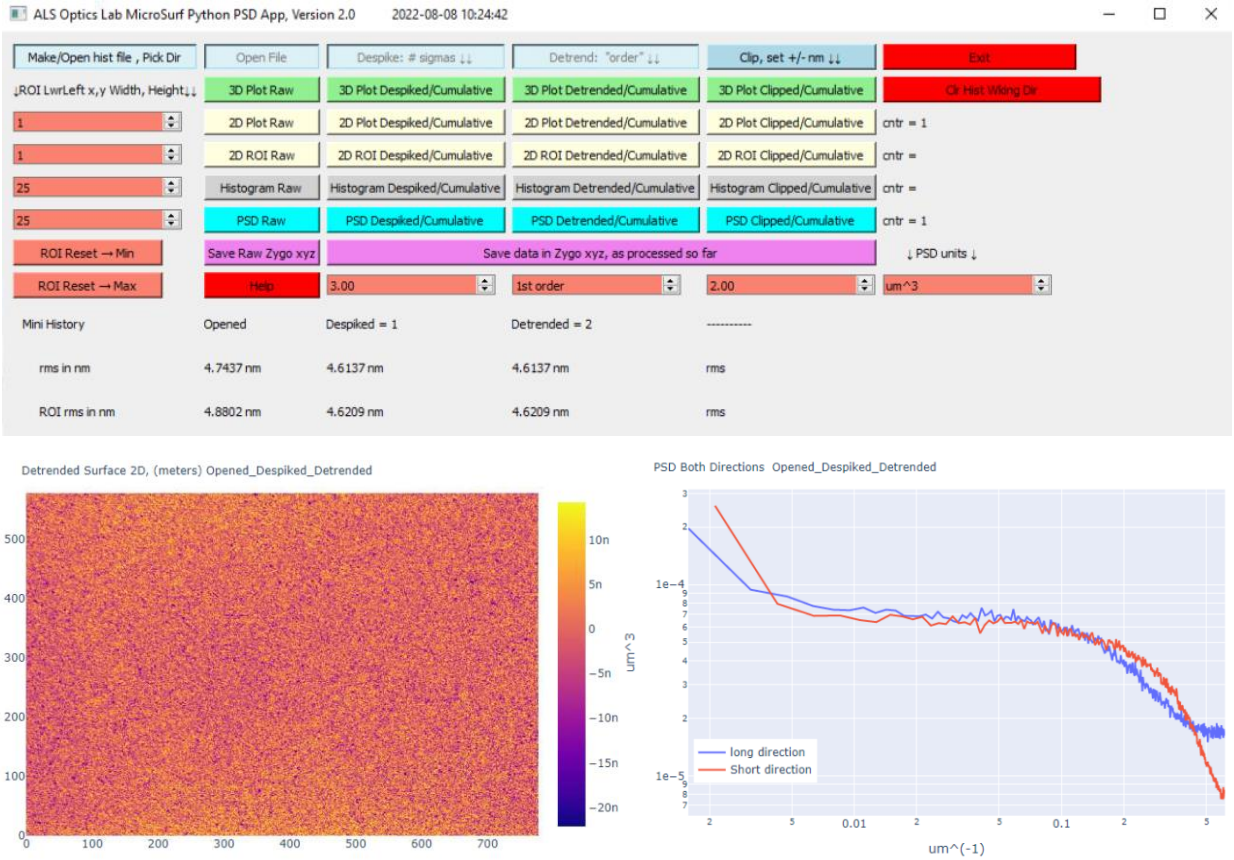

Figure 6. Screenshot of the developed data processing software as it appears in the course of the PSD evaluation based on the ITF calibration measurements with the BPRA standard in the experimental arrangement depicted in Fig. 2.

Basically, the GUI flows across the top in a series of blue widget buttons that allow the user to process the data from the 2-D array in the interferometric microscope in ways that are necessary to get a good PSD. Each widget button in the GUI calls a Python function that accomplishes the task, and returns control to the GUI when finished. First a working directory is chosen, and the history file is created for appending. Next the data are read in by the second blue widget button, and placed in a NumPy array [30]. An on-GUI record of each widget button that is pushed is kept as a log, both on screen, and in the history file.

The user next may choose the de-spike, detrend, and clip blue widget buttons in any order. The de-spiking is done by statistical replacement of points by a local average if they deviate more than a chosen number of sigmas from the average height of the surface. The user chooses this parameter in the salmon colored toggle-box widget at the bottom of the column of buttons. The default is 3.00 sigma. In any interferometric device that uses stepped phase measurements plus an algorithm to infer the height of a surface by calculation, there is always the chance that some data points may not solve properly. The de-spike function allows for the consideration of these points. For example, the previous MicroMap™ software would insert 10^(15) into non-computable pixels.

The second blue widget button across the top is for detrending. It is customary to remove low frequency undulations of the surface in question before computing the PSD. The most commonly used surface to remove is a generalized toric surface, expressed as a polynomial. It is the default. Planar, and cubic surfaces may also be chosen. Fully quartic surfaces were tried but did not converge with the fitting algorithm in use [31].

Finally, the data may be clipped. Certain artificial surfaces, such as binary pseudo-random arrays, created for calibration may need to have a floor and ceiling applied to the data. This is chosen in ±nm by the salmon colored data entry widget at the bottom of the column.

At any point in the process of using the blue widget buttons the data may be presented in graphical and numerical form by using the green, yellow, gray, blue, and violet widget buttons underneath each of the processing choices. The green widget buttons allow a 3-D plot of the data, as processed so far. Because the number of pixels in the array approaches a half million, the more common plotting packages were discarded in favor of Plotly [32]. matplotlib, while nearly universally used is insufferably slow for 3D graphs of even 50K points, taking about 5 minutes. PyQtgraph is much faster, but the 3D graphing methods are not fully mature, and not fully documented. Plotly has speed, terse syntax, and creates interactive 3D graphs quickly with large data sets. A decision was made mid-stream to remove the graphs from being displayed within the GUI, and make them automatically open in the default browser. taking advantage of one of the main features of Plotly. They are automatically saved in the chosen directory when created, explaining the total lack of "save the plot" buttons in the GUI. The 3D graphics are active, can be rotated, saved as scalable vector graphics files, and data can be read off from the figures.

The two yellow widget buttons beneath each blue widget button allow 2-D plots of the surface, as computed by the interferograms. Either the entire array of data is plotted by the top yellow widget, or a region of interest (ROI) can be plotted by the bottom of the two yellow widget buttons. The ROI is selected by start pixel, and width and height in pixels through salmon colored data input widgets on the left hand side of the GUI.

The gray widget buttons allow a histogram of the surface to be plotted. Histograms are very useful in following the results of the three main operators on the data. For example, they clearly show the effectiveness of the de-trending, and give insight into the statistical nature of the distribution of surface height values.

The blue buttons display the PSDs computed in both directions on the rectangular detector. They are averages of the line by line PSD. Two common units are selected by the salmon colored input widget box on the right hand side of the GUI. Finally, the violet widget buttons save the data, as computed so far, in a format which can be read by the other Zygo instruments that are in the ALS XROL.

Each graph plotted in html has the history of which widget calculations were performed written at the top of the graph. Each file has the history of which widget calculations were performed embedded in the filename of the saved file.

5. PERFORMANCE OF THE UPGRADED MICROSCOPE

To evaluate the performance of the upgraded microscope, we consider the stability of measurements, as well as the resolution capabilities.

A stability test (repeatability as the difference between identical acquisitions of image data) is free of specific aberrations of a particular objective or non-uniformity of the detector [33] and are ignored in favor of establishing the degree to which either can be characterized; via a reference surface file or calibration function. To examine the baseline stability of the instrument, we conducted repeat measurements of the surface of an x-ray mirror substrate, each with 128 exposure averages. The root-mean square (RMS) variation of the difference topography (Fig. 7), normalized by the factor of $2^{-1/2}$ for random, non-systematic error is ~ 0.8 Angstrom.

To determine resolution capabilities of the upgraded system, we use a highly randomized (HR) BPRA standard [23]. Where there are many HR-BPRA patterns available, with a range of elementary sizes of the binary pattern, and total number of elementary ‘pixels’ for this case we used the square ‘16k’ HR-BPRA pattern with 16,904 elements on a side, each of 241 nm elementary size. This filled the field of view of the 5x objective, while maintaining an elementary size below the diffraction limit for this white light interferometer. Data is recorded with single acquisition (no averaging) at a range of magnifications, Fig. 8. Where the inherent BPRA structure of the test part has a white-noise spatial frequency, any roll-off of the PSD of recorded data can be attributed to the instrument transfer function.

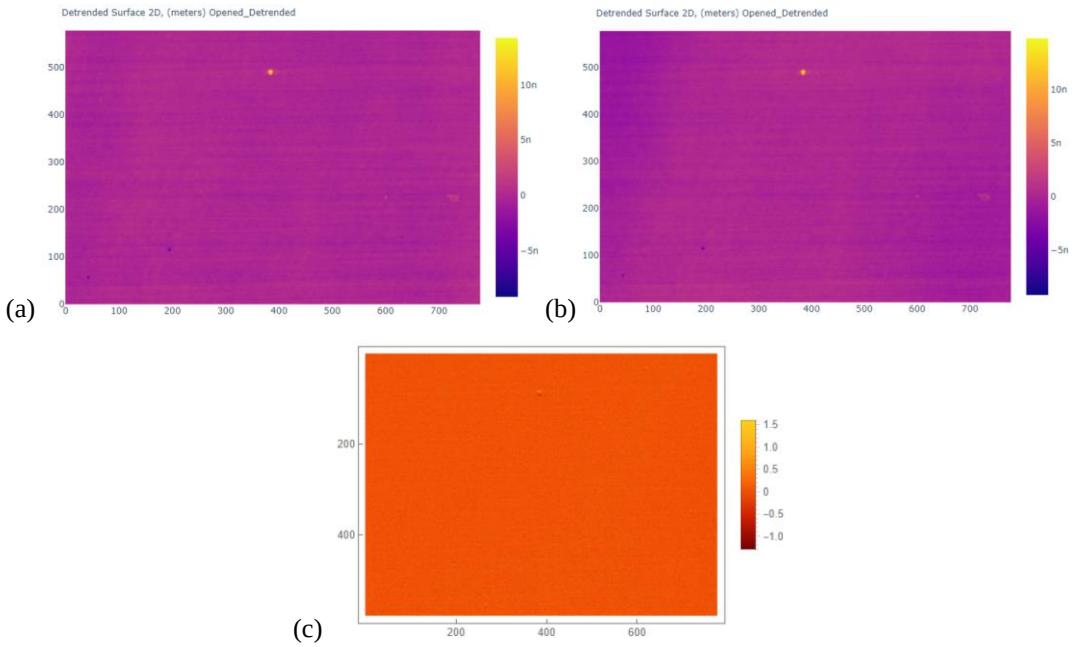

Figure 7. (a) and (b) Two sequential measurements with the upgraded microscope with the 20x Objective and (c) the difference of the measurements as a measure of the precision of the surface topography metrology achieved with the upgraded MicroMap/OptoSURF microscope. The root-mean square (RMS) variation of the difference topography, normalized by the factor of 2-1/2 is ~ 0.7 Angstrom.

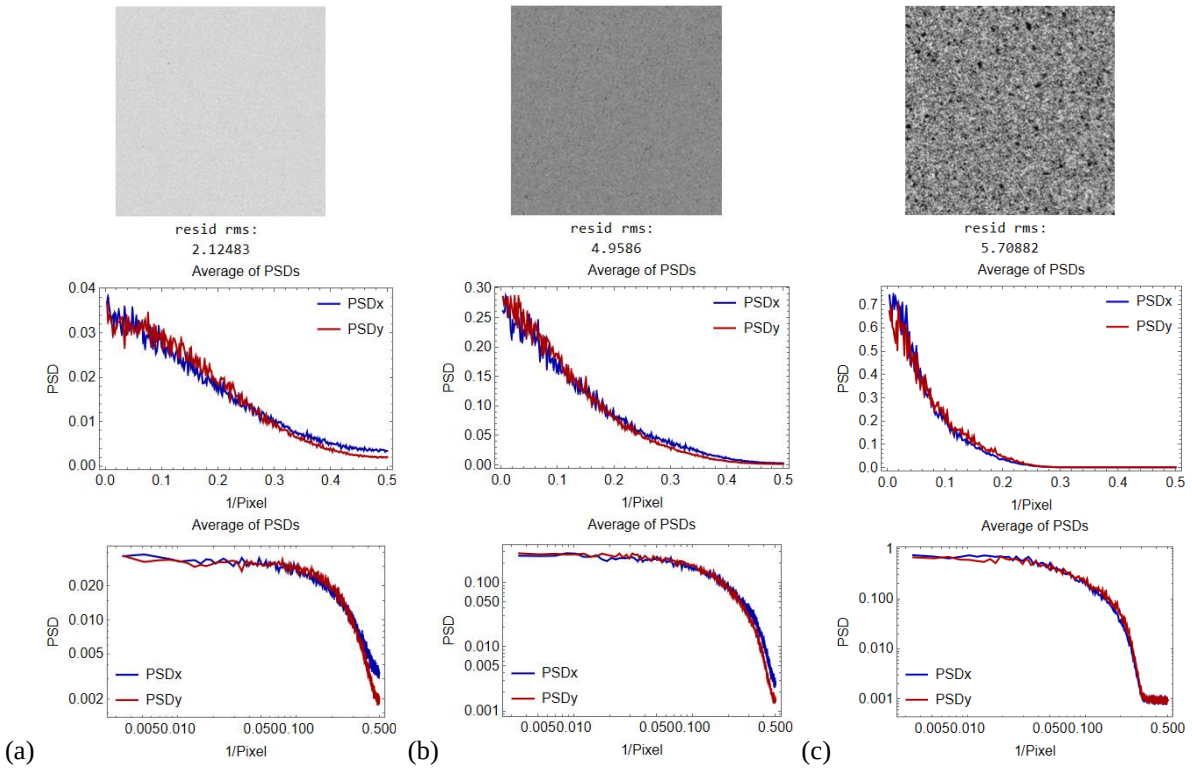

Figure 8. For three objectives, 5x (a), 20x (b), and 50x (c), greyscale representation of measurements of the HR-BPRA test part (top), with the average of the x-direction and y-direction RSDs shown in two scales, Linear (center), and log (bottom). The asymmetry of the PSDs in the x and y direction indicate that the x direction is more stable and therefore has better resolution capabilities.

For an additional consideration of the mechanical performance stability, we consider the asymmetry of the x and y direction PSDs from measurements of the BPRA test part. Where the x direction of the detector is along the tangential direction of x-ray optics placed on the stage, and this is the more stable direction, this validates the arrangement of the system.

6. DISCUSSION AND CONCLUSIONS

X-ray optics and optical systems, with strong asymmetric form factors given the grazing incidence beamline applications with world leading surface quality requirements pose a challenge for metrology systems. While may new microscope systems are available on the market, they are generally configured for relatively small samples. We have demonstrated the feasibility of refurbishing and improving a legacy instrument with dynamic functionality.

In the process, we joined commercial component upgrades, with a custom stage that utilizes off the shelf motors allowing fault-tolerant longevity, and in the process supported the next generation of researchers through a directed outreach internship program [34]. The upgraded system allows remote operation so that the environment inside the instrument hutch does not need to be disturbed for realignments during the course of measurements.

Custom software has been developed to allow file format conversion for a variety of other post processing analysis, as well as dedicated spatial frequency processing that records the specific pre-processing, such as spike clipping and detrending parameters for unambiguous interpretation of results.

The upgraded system is capable of providing sub-Angstrom surface height measurements for large x-ray optical surfaces. This even for challenging arrangements, e.g. mounted assemblies, or substrates with unwieldy flanges.

ACKNOWLEDGEMENTS

Research at the Advanced Light Source Engineering Division at Lawrence Berkeley National Laboratory is supported by the Office of Science, Office of Basic Energy Sciences, and Material Science Division of the U.S. Department of Energy under Contract No. DE-AC02-05CH11231.

The ASPIRES (Advancing STEM Pioneers In Research in Energy Sciences) Internship Program, Summer (2022), supported the work of our intern, Muhammad A. Saeed, who helped realize the instrumentation upgrade.

DISCLAIMER

REFERENCES

[1] Takacs, P. Z. and Church, E. L. “Figure and Finish of Grazing-incidence Mirrors,” Nucl. Instrum. and Meth. A291, 253-264 (1990); https://doi.org/10.1016/0168-9002(90)90071-D.

[2] Church, E. L. and Takacs, P. Z., “Surface Scattering,” in [Handbook in Optics], Vol. 1: Classical Optics, Vision Optics, X-Ray Optics, M. Bass, Jay M. Enoch, E. W. Van Stryland, W. L. Wolfe eds., 2nd Ed., McGraw-Hill Inc., New York, Ch. 7 (2000).

[3] Assoufid, L., Hignette, O., Howells, M., Irick, S., Lammert, H., and Takacs, P. Z., “Future metrology needs for synchrotron radiation grazing-incidence optics,” Nucl. Instrum. and Meth. A 467-468, 267-270 (2001); https://doi.org/10.1016/S0168-9002%2801%2900296-0.

[4] Freund, A. K., "Challenges for synchrotron X-ray optics," Proc. SPIE 4782, 1-11 (2002); https://doi.org/10.1117/12.455685.
[5] Yashchuk, V. V., Samoylova, L., and Kozhevnikov, I. V., "Specification of x-ray mirrors in terms of system performance: new twist to an old plot," Opt. Eng., 54(2), 025108 (2015); doi:10.1117/1.OE.54.2.025108.
[6] Creath, K. and Wyant, J., "Absolute measurement of surface roughness," Appl. Opt., 29, 3823–3827 (1990); doi: 10.1364/AO.29.003823.
[7] Saxer, C. and Freischlad, K., "Interference microscope for sub-Angstrom surface roughness measurements," Proc. SPIE 5144, 37-45 (2003); https://doi.org/10.1117/12.500925.
[8] Iles, S. and Nelson, J., "Sub-Angstrom surface roughness metrology with the white light interferometer," Proc. SPIE 11175, 1117519/1-12 (2019); doi: 10.1117/12.2536683.
[9] Leach, R., Ed., [Optical Measurements of Surface Topography], Springer-Verlag, Berlin & Heidelberg (2011).
[10] de Groot, P., "Principles of interference microscopy for the measurement of surface topography," Adv. Opt. Photon. 7, 1-65 (2015), doi:10.1364/AOP7.000001.
[11] Shvyd'ko, Y., [X-Ray Optics: High-Energy-Resolution Applications], Springer-Verlag, Berlin & Heidelberg (2004).
[12] Attwood, D. and Sakdinawat, A., [X-Rays and Extreme Ultraviolet Radiation], 2nd Ed., Cambridge University Press, New York (2016).
[13] Yashchuk, V. V., Artemiev, N. A., Lacey, I., McKinney, W. R., and Padmore, H. A., "A new X-ray optics laboratory (XROL) at the ALS: Mission, arrangement, metrology capabilities, performance, and future plans," Proc. SPIE 9206, 92060I/1-19 (2014); doi:10.1117/12.2062042.
[14] Yashchuk, V. V., Artemiev, N. A., Lacey, I., McKinney, W. R., and Padmore, H. A., "Advanced environmental control as a key component in the development of ultra-high accuracy ex situ metrology for x-ray optics," Opt. Eng. 54(10), 104104 (2015); doi: 10.1117/1.OE.54.10.104104.
[15] Yashchuk, V. V., Irick, S. C., Gullikson, E. M., Howells, M. R., MacDowell, A. A., McKinney, W. R., Salmassi, F., Warwick, T., "Cross-check of different techniques for two-dimensional power spectral density measurements of X-ray optics," Proc. SPIE 5921, 59210G/1-12 (2005); https://doi.org/10.1117/12.619892.
[16] Yashchuk, V. V., Franck, A. D., Irick, S. C., Howells, M. R., MacDowell, A. A., McKinney, W. R., "Two dimensional power spectral density measurements of X-ray optics with the Micromap interferometric microscope," Proc. SPIE 5858, 58580A/1-12 (2005); https://doi.org/10.1117/12.612383.
[17] Yashchuk, V. V., Gullikson, E. M., Howells, M. R., Irick, S. C., MacDowell, A. A., McKinney, W. R., Salmassi, F., Warwick, T., Metz, J. P., and Tonnessen, T. W., "Surface Roughness of Stainless Steel Mirrors for Focusing Soft X-rays," Appl. Opt. 45(20) 4833-4842 (2006); https://doi.org/10.1364/AO.45.004833.
[18] https://eotech-sa.com/metrology/surface-characterization/optosurf/
[19] Yashchuk, V. V., McKinney, W. R., and Takacs, P. Z., "Test surfaces useful for calibration of surface profilometers," United States Patent No.: 8,616,044.
[20] Yashchuk, V. V., McKinney, W. R., and Takacs, P. Z., "Binary pseudorandom grating as a standard test surface for measurement of modulation transfer function of interferometric microscopes, Proc. SPIE 6704, 670408 (2007); https://doi.org/10.1117/12.732557.
[21] Yashchuk, V. V., McKinney, W. R., and Takacs, P. Z., "Binary pseudorandom grating standard for calibration of surface profilometers," Opt. Eng. 47(7), 073602-1-5 (2008); https://doi.org/10.1117/1.2955798.
[22] Munechika, K., Rochester, S., Chao, W., Lacey, I., Pina-Hernandez, C., and Yashchuk, V. V., "Binary pseudo-random array standards for calibration of 3D optical surface profilers used for metrology with aspheric x-ray optics," SPIE Optics and Photonics 2022, Conference OP323: Interferometry XXI, Paper No.: OP323-16; Tracking No.: OP22O-OP323-16 (San Diego, August 21-25, 2022); this conference.
[23] Yashchuk, V. V., Munechika, K., Rochester, S., Chao, W., Lacey, I., Pina-Hernandez, C., and Takacs, P. Z., "Reliability investigation of the instrument transfer function calibration technique based on binary pseudo-random array standards," SPIE Optics and Photonics 2022, Conference OP501: Advances in Metrology for X-Ray and EUV Optics X, Paper No.: 12240-25; Tracking No.: OP22O-OP501-4 (San Diego, August 21-25, 2022); this conference.
[24] Griesmann, U., Munechika, K., Renegara, T. B., Zheng, X. A., Soons, J. A., Chao, W., Lacey, I., Pina-Hernandez, C., Takacs, P. Z., and Yashchuk, V. V., "Characterization of surface texture-measuring optical microscopes using a binary pseudo-random array standard," SPIE Optics and Photonics 2022, Conference OP323: Interferometry XXI, Paper No.: OP323-21; Tracking No.: OP22O-OP323-21 (San Diego, August 21-25, 2022); this conference.
[25] Takacs, P. Z., Rochester, S., Lacey, I., Munechika, K., and Yashchuk, V. V., "Calibration, modeling, parameterization, and verification of the Instrument Transfer Function of an interferometric microscope," SPIE Optics and Photonics

2022, Conference OP323: Interferometry XXI, Paper No.: OP323-13; Tracking No.: OP22O-OP323-13 (San Diego, August 21-25, 2022); this conference.
[26] http://americanlinear.com/html/sr_series_stages.html
[27] https://www.thorlabs.com/newgrouppage9.cfm?objectgroup_id=1881&pn=DRV208#2544
[28] Elson, J. M. and Bennett, J. M., "Calculation of the power spectral density from surface profile data," Appl. Opt. 34(1), 201-208 (1995); https://doi.org/10.1364/AO.34.000201.
[29] Limited, R. C. (2022). PYQT5, https://pypi.org/project/PyQt5/.
[30] Ecosystem (2022). NumPy, https://numpy.org/.
[31] MIT (2022). https://pypi.org/project/symfit/
[32] Enterprise, D. (2022). Plotly, https://plotly.com/.
[33] Rochester, S, English, D, Lacey, I, Munechika, K, Yashchuk, V. V., "Towards super-resolution interference microscopy metrology of x-ray variable-line-spacing diffraction gratings: Recent developments," SPIE Optics + Photonics 2022, Paper No. 12240-26, Tracking No.: OP22O-OP501-5; this conference.
[34] ASPIRES (Advancing STEM Pioneers In Research in Energy Sciences) Internship Program, Summer (2022), https://sites.google.com/lbl.gov/esaintern/projects/2022-program-projects.